Materials Research Proceedings 28 (2023) 505-514 https://doi.org/10.21741/9781644902479-55

Investigations into the processing and texture of Pr-substituted NdFeB magnets produced by extrusion

RÜDIGER Alexander[1,a *], GALL Sven[2,b] and MÜLLER Sören[1,c]

[1]Extrusion Research & Development Center, Technische Universität Berlin, Gustav-Meyer-Allee 25, 13355 Berlin, Germany

[2]INGWERK GmbH, Rohrdamm 88, 13629 Berlin

[a]a.ruediger@tu-berlin.de, [b]sven.gall@ingwerk.com, [c]soeren.mueller@tu-berlin.de

Keywords: Pr/NdFeB, Anisotropic Magnets, Extrusion, Hot Deformation

Abstract. Crystallographically and magnetically textured but dimensionally limited NdFeB permanent magnets produced by hot deforming processes such as die-upsetting and back-extrusion have been extensively researched in the past [1]. In order to investigate the possibility of producing longer magnets which can subsequently be cut to the required length, the extrusion of permanent magnets was investigated as a further hot deformation process. For this purpose, the process control with regard to the tools used as well as the process parameters were modified from the common forming processes for extrusion. Therefore, a praseodymium-substituted NdFeB powder was encapsulated in steel and extruded by varying the extrusion ratio (9.9:1 & 13.9), the billet insert temperature (800°C & 850°C) and the extrusion speed (0.6 - 10.5 mm/s). In addition, the glass lubrication system was changed during the experiments. Since the resulting magnetic properties for hot deformation depend on the produced anisotropy, texture analyses were also carried out in the first step by means of X-ray diffraction on the cross-sections of the produced strands. For the parameter variation, strands could be realized with the applied concept. However, cracks were found in the magnetic material for all tests. Based on the texture analyses, anisotropy could be generated in the magnet material for all strands.

Introduction

Permanent magnets based on NdFeB are widely used in further areas due to their excellent magnetic properties in the form of high energy product $(BH)_{max}$. For anisotropic magnets, this is based on an alignment of the hard magnetic $Nd_2Fe_{14}B$ phase during the manufacturing process. In addition to the sintering route, in which a magnetic field must be applied during the manufacturing process for alignment, anisotropy can also be achieved by hot deformation (Figure 1). The advantage of this is that no magnetic field is required [1]. In order to improve the coercivity of sintered magnets, neodymium is often substituted in parts with dysprosium in many alloys. However, this is characterized by low availability and a high price. As a further substitution variant, it is possible to add praseodymium to the powder alloys without strongly affecting the magnetic properties. The lower purchase price compared to neodymium plays a decisive role in this case [2-4]. Another approach to improve the coercivity is to keep the grain size of the magnets as small as possible [5,6]. Due to the production method of the powder for the hot- deformation processes, these are especially distinguished for this purpose.

Here, the magnetic powders for further processing are produced by the melt-spinning process. In this, the molten starting material is applied to a wheel at high rotational speeds. The material spun off undergoes very rapid cooling and grain sizes in the sub-µm range are achieved. In the final powder, the grains are present in the platelet-shaped particles without crystallographic preferred orientation. Die-upsetting and back-extrusion are two forming processes that have already been intensively researched and applied in practice [1,7]. They can be used to produce

block magnets or ring magnets with high magnetic properties. As already mentioned, these high magnetic properties are based on the formation of a suitable texture by hot-deforming. In the die-upsetting example, the powder is first hot compacted. This step is carried out in an argon atmosphere, since the powder tends to oxidize at the high operating temperatures. The pre-compacted blank is then hot-deformed. In this process, the formation of anisotropy is based on the fact that a liquid phase is formed at the grain boundaries and the grains undergo preferential grain growth in the a-axis direction of the tetragonal NdFeB unit cell. The grain growth is thereby fed by diffusion processes in the liquid phase [8-12]. Fig. 1 compares the manufacturing processes for sintered magnets and for the hot-deformed magnets (die-upsetting and back-extrusion) with the manufacturing approach studied in the experiments. In addition, the anisotropy achieved for the hot-deformed magnets is shown based on the C-axis orientation of the $Nd_2Fe_{14}B$ phases.

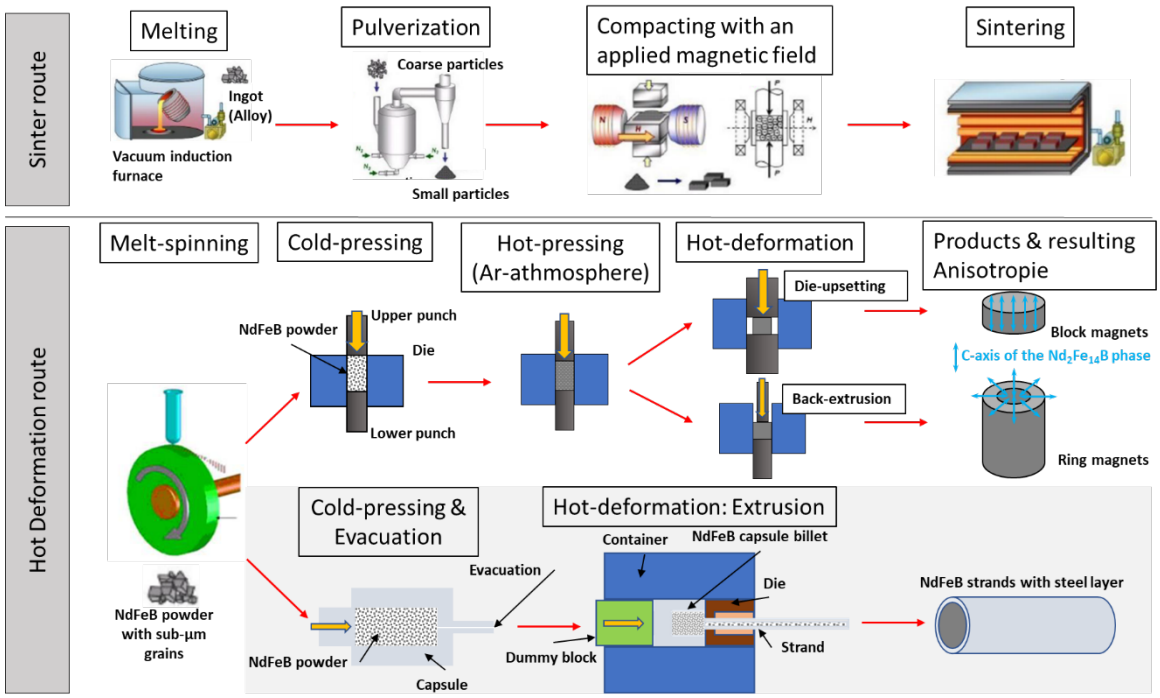

Fig. 1. Manufacturing processes of NdFeB magnets via sintering and hot-deformtion as well as the chosen investigation approach via extrusion [13].

The present investigations are intended to provide initial information on the conditions under which the extrusion of Pr/NdFeB is possible. For this purpose, in contrast to die-upsetting, the process control is adapted in such a way that pre-compaction at high temperatures is avoided and the powder is thus pressed directly. In order to obtain a first impression of the magnetic properties, texture measurements are carried out on the samples according to the correlation between these and the anisotropy achieved in the material.

Experimental Procedure

A Dy-free powder alloy with Nd substituted by Pr was used for the tests. The alloy composition is shown in Table 1. This was produced by the company Magnequench by means of the melt-spinning process for further processing by hot-deformation. Furthermore, Table 1 shows the particle size distribution of the powder used.

Table 1. Alloy composition and particle size distribution of the powder used.

element	Nd	Pr	Dy	B	Co	Ga	Fe
[ICP%]	7,80	22,60	0,00	0,88	3,90	0,49	64,33
Particel sizes by mesh & max. diameter	**>40 >425 µm**	**>60 >250µm**	**>100 >150µm**	**>200 >75µm**	**>325 >53µm**	**>375 >45µm**	**<375 <45µm**
[wt.%]	0,0	19,7	40,1	27,5	4,8	1,4	6,5

Direct extrusion was selected as the process for hot-deforming. For this, the set-up shown in Fig. 2 consisting of die (Hot work tool steel 1.2367) with ceramic ring insert (Al2O3), inlet ring (1.2367) with half die angle of α = 60°, glass pad, evacuated capsule billet with applied glass lubrication (slurry) and dummy block (1.2367) in a container with a diameter of 85 mm was used. The extrusions were carried out on the 8 MN extrusion press of the Extrusion Research & Development Center (TU Berlin).

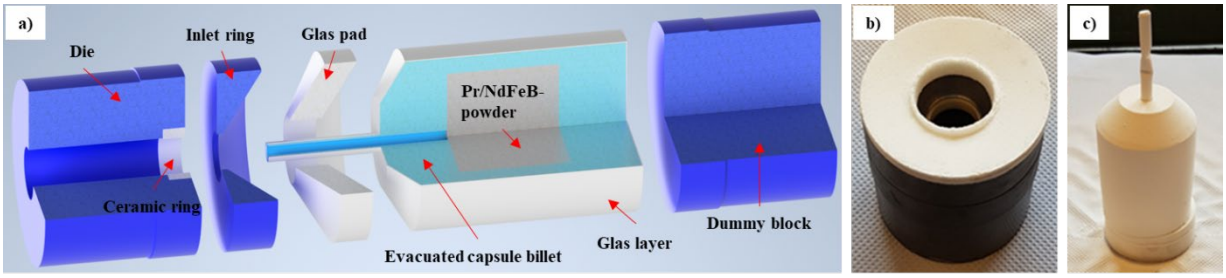

Fig. 2. a) Illustration of the experimental setup; b) Assembly of die, ceramic ring, inlet ring and glass pad; c) evacuated capsule billet with glass layer.

The powder was extruded in the encapsulated and evacuated form shown above, since the powder tends to oxidize at the forming temperatures applied. Accordingly, a capsule was first manufactured from mild steel (1.0577) with an outer diameter of 80 mm and a wall thickness of 8 mm, and then filled with the powder. In order to increase the output, the powder was also cold pre-compacted before evacuation. Furthermore, a two-part glass-based lubrication system, consisting of a glass pad and a glass layer sprayed onto the billet, was used for the extrusions. The purpose of this is to minimize friction and provide thermal insulation against the tools (container, die with ceramic ring, inlet ring and dummy block). The operating temperature of the mentioned tools was set to 500°C for the experiments. In the direct extrusion process used, the NdFeB billet together with the capsule material is pressed through the die by the dummy block and tapered to form a strand. Here, the inlet ring serves to improve the material flow into the deformation zone. The final cross-sectional geometry of the strand is determined by the ceramic ring, which represents the bearing channel of the die. In the best case, this remains intact throughout the entire extrusion.

For the tests, the billet operating temperatures, the diameter of the bearing channel, the ram speed and the type of glass lubrication system (Reimbold & Strick Handels- und EntwicklungsGmbH) used were varied (Table 2).

Table 2. Used experimental parameters.

	Billet operating temperature [°C]	Diameter oft he bearing channel [mm]	Extrusion ratio [-]	Ram speed [mm/s]	Glass lubrication system with application temperature range
#1	800	27	9,9:1	8,8	Pad: RS2745 0,1-0,4 (780 °C -1140 °C) Slurry: RS2745/10,063 (780 °C -1140 °C)
#2	800	22,8	13,9:1	10,5	as in #1
#3	850	22,8	13,9:1	8,7	as in #1
#4	850	22,8	13,9:1	6,8	as in #1
#5	850	22,8	13,9:1	4,8	Pad: NP7595 0,1-0,4 (620 °C -1000 °C) Slurry: GO12649 (620 °C -1000 °C)
#6	850	22,8	13,9:1	0,6	as in #5

For the qualitative investigations of the extruded strands, visual inspections of the strands were carried out on the one hand, and metallographic analyses in the form of X-ray diffraction (XRD) were performed on strand cross-sections to show the obtained textures on the other hand. When preparing the samples for XRD analyses, they were first grounded with a grit size of 4000 and then polished with diamond suspensions at 6 µm, 3 µm and 1 µm levels. The texture measurements were performed on the polished cross-sections of the strands in the center and in the edge region of the magnetic material. The measurements were carried out at the Department of Metallic Materials at the TU Berlin on a diffractometer from the Huber company using a location-sensitive detector OED 50 M from M. Braun GmbH. These involved monochromatic Co-Kα radiation (λ = 0.17887 nm), an accelerating voltage of 40 kV, a current of 25 mA, and a collimator with a diameter of 1 mm, and the crystal orientations {004}, {310}, {313}, {410}, {411}, and {006} were measured. For the measurements, the samples were rotated azimuthally (φ) in 5° steps from 0° to 355° and repeated for tilt angle steps (Ψ) of 5° ranging from 0° to 55°. The program MTEX was used to determine the orientation distribution functions (ODF) and create the pole figures.

Results and Discussion

Fig. 3 shows the resulting strands of the test extrusions. It can be seen that for all test parameters, strands could be extruded which also contain magnetic material. In addition, Table 3 summarizes the extrusion forces measured during the tests as a function of the stepwise parameter adjustments. The total force to be applied by the extrusion press is the sum of the die force and the friction force. The forces are determined by load cells which are coupled to the container for the friction force and to the die for the die force. In the case of the used container (diameter of 85 mm), the total force is also restricted to 6.5 MN in order to avoid exceeding the critical yield stresses of the used tools.

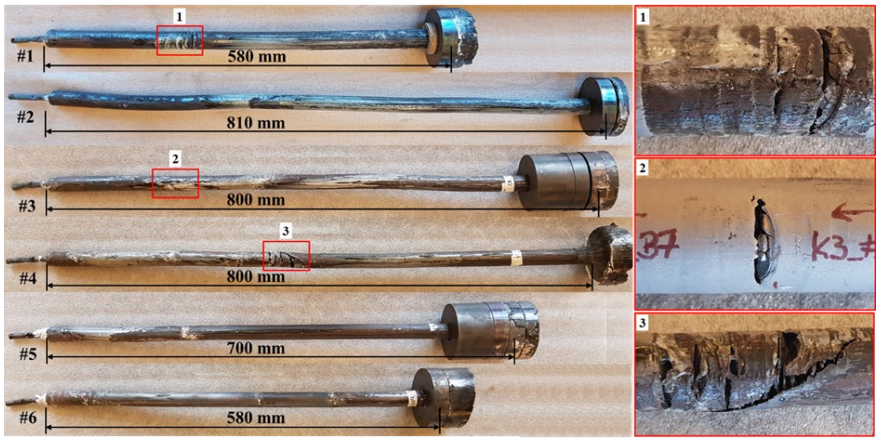

Fig. 3. Strands of tests No. 1 to No. 6 (left); 1-3) Pressing defects.

Table 3. Measured extrusion forces as function of the stepwise parameter adjustments.

	#1	#2	#3	#4	#5	#6
Parameter adjustments		Increased extrusion ratio Increase Ram Speed	Increased billet Temperatur Decreased Ram speed	Decreased Ram speed	Changed Glass lubrication system Decrease Ram speed	Decrease Ram speed
Die Force [MN]	4,1	4,9	4,8	5,1	4,4	4,0
Friction Force [MN]	1,0	1,3	1,5	1,2	0,4	0,3
Total force [MN]	5,1	6,2	6,3	6,3	4,8	4,3

For test No. 1, the required die force and the friction force between billet and container were measured to be 4.1 MN and 1.0 MN, respectively. By increasing the ram speed and decreasing the bearing channel diameter, the die force increased as expected to 4.9 MN. The friction force was measured at 1.3 MN, resulting in a total force of 6.2 MN to be provided by the extrusion press. This results in very high stresses for the ram and the used tools. To counteract these, the billet operating temperature was increased and the extrusion speed reduced for test No. 3. However, despite the adjustments, 4.8 MN and 1.5 MN were measured for the die and friction forces, respectively. It can be assumed that the adjustment of the extrusion speed is not sufficient to achieve sufficiently high differences in the mean logarithmic forming speeds which can be calculated according to the formula [14]:

$$\underline{\dot{\varphi}_g} = \frac{(V-1)\cdot 2\cdot tan\alpha}{D_0 \cdot D_S} \quad (1)$$

Here V is the extrusion ratio, α is the die angle, D_o is the container diameter and D_s is the strand diameter. The determined small reduction from 7.5 1/s to 6.3 1/s could therefore not be sufficient to achieve a relevant reduction in the flow stresses of the material. For test No. 4, the ram speed was further reduced. Here, too, no relevant deviations from the values of test No. 2 could be observed with 5.1 MN and 1.2 MN. This could equally be attributed to a still slight reduction of the mean logarithmic forming speed to 4.9 1/s. In addition, it could be considered for the tests that manual loading oft he billet can lead to delays in the extrusion process.

This means that even short time differences can lead to strong cooling of the billet due to the high temperature gradient between the container and the billet, which can also lead to an increase in the flow stresses in the deformation zone. In order to further reduce the forces, a new lubrication system suitable for use at lower temperatures was used for tests No. 5 and No. 6. At the same time, the ram speed was further reduced for test No. 5. As a result, the die and friction forces were significantly reduced to values of 4.4 MN and 0.4 MN, respectively. The reduction in the friction force, which is measured by load cells attached to the container, can thus be attributed to the reduced friction between container and billet surface. The lower die force can also be explained by a reduction in friction. In this case it is due to the reduced friction between the billet and die, since the measured values for the forming force are recorded via load cells on the die, i.e. decoupled from the friction force. The improved material flow at the die, i.e. facilitated by the more suitable lubrication system, also improves the formability. For test No. 6, a further reduction in the ram speed also resulted in lower values for the die and friction forces of 4.0 MN and 0.3 MN in the steady-state of extrusion. In contrast to the previous tests, however, this billet could not be extruded completely, which resulted in an increase in the total force to a maximum acceptable value of 6.5 MN for the test setup, above which forming was no longer achieved with the corresponding extrusion force. In this case, it can be assumed that the set low ram speed during the extrusion results in excessive cooling of the billet and thus freezing of the billet. Figure 3 also

Materials Research Proceedings 28 (2023) 505-514 https://doi.org/10.21741/9781644902479-55

shows the strand lengths obtained. For tests No. 1 to No. 5, the theoretical lengths calculated via the volume consistency (approx. 600 mm for ER. 9.9:1; approx. 800 mm for ER. 13.9:1) could be achieved, whereby the deviating strand length for test No. 5 is due to a shortened capsule cover of 10 mm. In accordance with the not completely extruded billet in test No. 6, a reduced strand length of 580 mm was realized here. Also extrusion defects for strands No. 1, No. 3 and No. 4 are shown in Figure 3. These are cracks in the shell material of the strand areas with magnetic core, which are perpendicular to the extrusion direction. The magnet material in these areas is also characterized by strong transverse cracks, in some cases also beyond the areas of the shell cracks (see Figure 3, detail view 2). Figure 4 shows the theoretical positions of the magnet material as well as the real cutting positions for removing the relevant magnet areas in the resulting strands for the two different extrusion ratios. The strand sections shown in Figure 5 were extracted according to these cutting positions. For reasons of equivalence with respect to strand No. 2, strands No. 3 and No. 4 are not shown.

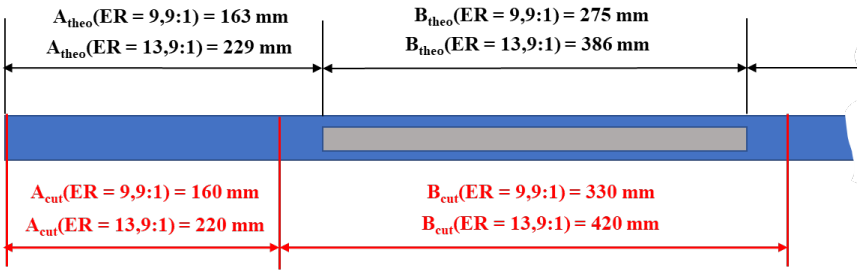

Fig. 4. Theoretical position of the magnetic material in the strand (black); removal positions for the magnetic material (red).

In addition, Fig. 5 shows the sections through the magnet-filled areas in order to compare them with the theoretical material flow.

While for the experiments No. 1 to No. 5 the section lengths of 330 mm and 420 mm given in Fig. 4 were observed due to the complete extrusion of the billets, only a section of 340 mm could be taken for experiment No. 6. The cross-sections also show that the magnetic material is present in different proportions over the length of the sections. Thus, for all tests, there is a pronounced back-end defect at the end of the section, in which the capsule bottom material flows forward in the middle of the strand and the magnetic material is therefore present in a ring shaped area in the cross-section. On the other hand, a variable area fraction of the magnetic material can also be seen in the areas without back-end defect, whereby this decreases over the extrusion. In the case of tests No. 5 and No. 6, it can be seen that magnetic material is already present in the strand before the theoretically determined position. In the case of test No. 5, it can be assumed that the shortened capsule cover is the cause of the displaced position of the magnet. In the case of test No. 6, it could be assumed that, due to the low extrusion speed, the flow stresses for the steel are higher than for the magnet material as a result of the rapid cooling of the billet. This would result in a pre-flow of the magnet material in the center of the strand. Furthermore, in Fig. 5, cracks can be seen in the magnet material along the entire strand length for all tests, not just in the defect areas shown in Fig. 4. On the one hand these could be explained by insufficient matching of the forming properties of the material composite and on the other hand by the difference in the thermal expansion coefficients of the two materials.

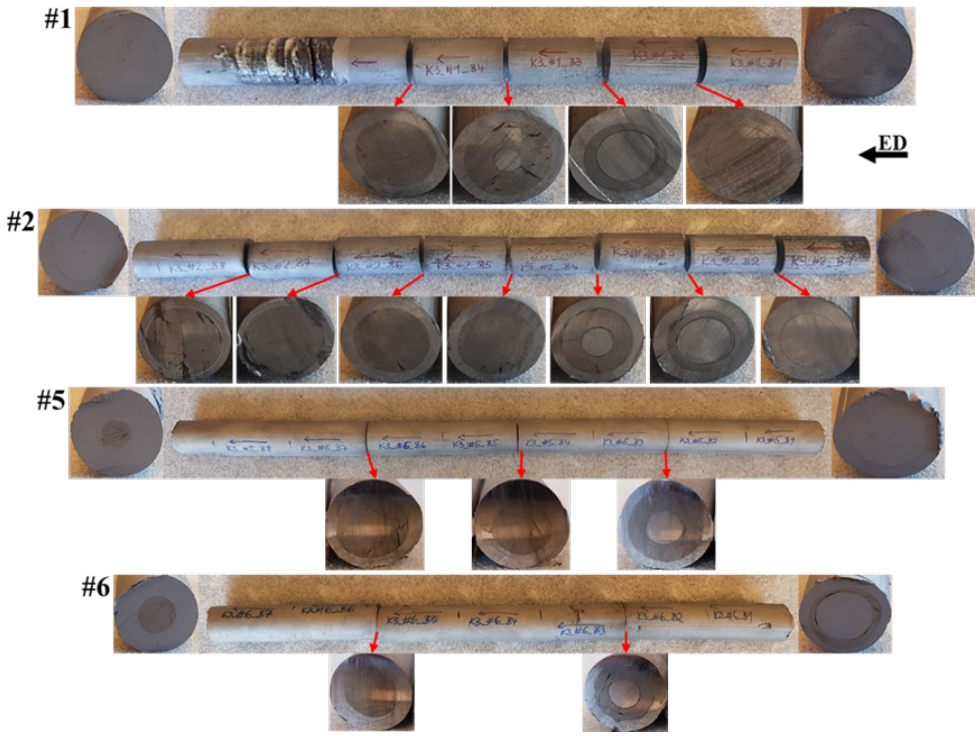

Fig. 5. Resulting strands and strand cross sections.

Fig. 6 shows the pole figures determined by XRD for selected tests at the edge and in the center of the magnetic material. For the investigations, sample cross-sections were considered in which the area fraction of the magnetic material was the largest. Since the pole figures for tests No. 2 to No. 5 do not show any decisive differences, these are represented for the edge by test No. 2 and for the center by test No. 3.

In general, an orientation of the lattice structure can be determined for all tests, both at the edge and in the center, in which the (002) planes are preferably perpendicular to the cross-sectional plane and rotated with respect to the extrusion direction. The (100) planes are primarily oriented in the cross-sectional plane or perpendicular to it. According to these orientations, the (110) planes are thus preferably rotated by 45° to the orientation of the (100) planes, as can be seen in Fig. 6. Furthermore, it can be seen that a certain proportion of the (001) planes are oriented horizontally in the cross-sectional planes, especially in the measuring positions at the edge. This indicates that an theoretically expected anisotropy is more pronounced in the center regions. In theory, the hot-deforming of Pr/NdFeB results in an anisotropy in which the (002) planes are perpendicular to the applied pressure direction. This can be seen in the die-upsetting and back-extrusion processes (Fig. 1). Consequently, in the process used here, a radial orientation of the c-axes of the tetragonal unit cell, corresponding to the anisotropy in back-extrusion magnets, would ideally be expected in the cross-sectional area of the strand.

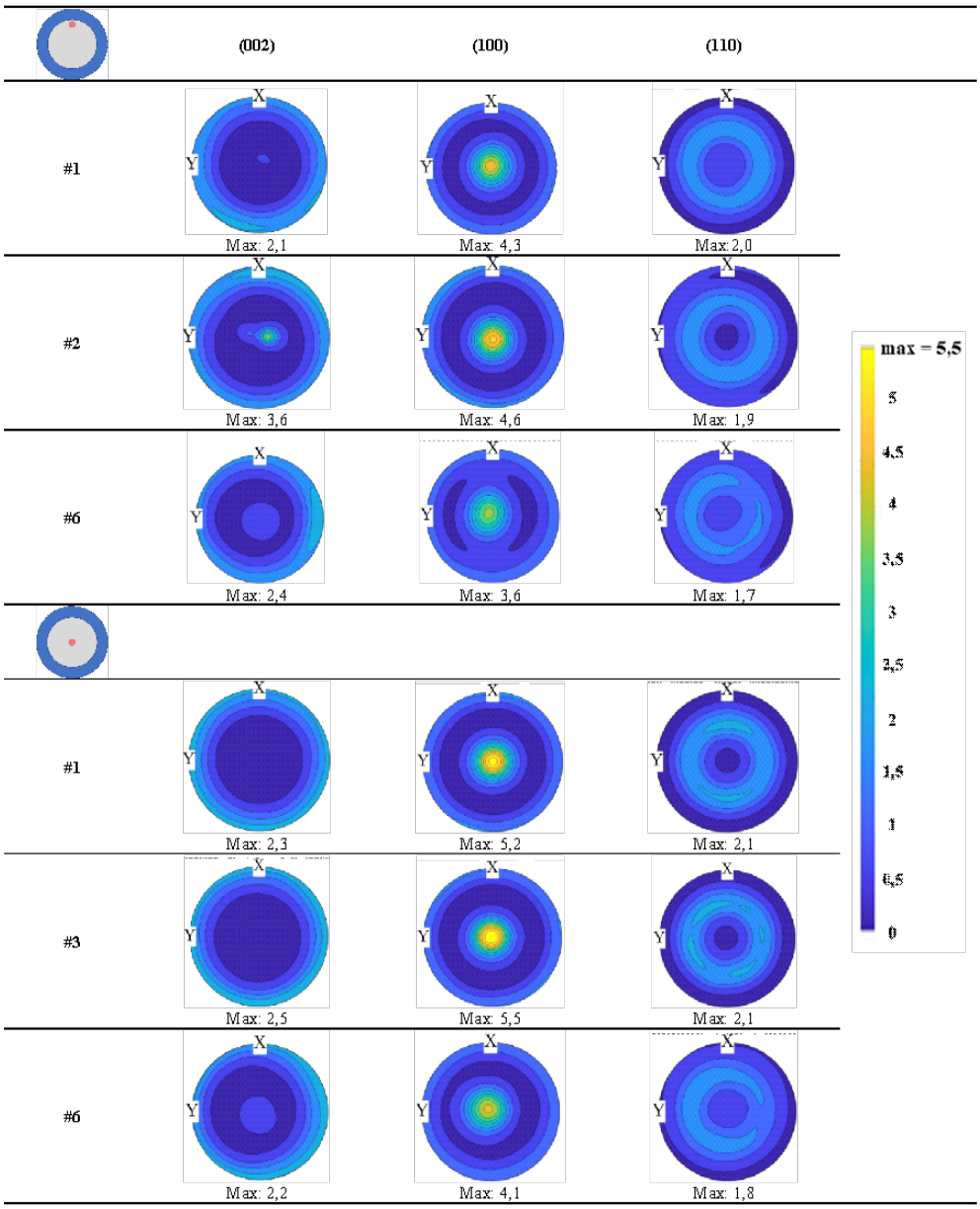

Fig. 6. Pole figures determined by XRD at the edges and in the center of the strands; the colored legend represents the intensity range of the displayed pole figures.

For the occurrence of the perpendicular to the extrusion direction orientated (002) planes in the edge region, it can be assumed that, due to too rapid cooling of the magnetic material, no sufficient rotation of the grains in the liquid phase required for hot deformation is possible at the extrusion speeds used because of the large temperature gradient between the container and the billet. Consequently, the temperatures in this area could drop too quickly into the temperature range of the solidifying temperature of the liquid phase. A similar argument can be made for test No. 6 in the center of the strand. Here, the possibly too slow pressing speed for the experimental setup could lead to a rapid cooling of the billet down to the center of the material and thus cause the observed superimposed anisotropy. Furthermore, it can be assumed that the not achieved radial anisotropy can be explained by insufficient shear of the material based on the possibly too low selected extrusion ratios. In general, it should be noted that for further tests to optimize the

anisotropy, the tools must be adapted with regard to realise a constant Temepratur in the billet over the entire extrusion.

Summary

With the selected test setup for direct extrusion of encapsulated magnetic powder, strands with magnetic material or at least partial strands (Test No. 6) could be processed for all parameters. A pronounced back-end defect was observed for all strands. For some strands, partial cracks of the strand shell and and in these areas strong cracks in the magnetic material perpendicular to the extrusion direction could be observed. In addition, the magnet material was riddled with finer cracks in all tests. In future, consideration can be given here to adapt the capsule material in order to better match the flow properties to the magnet material in the temperature range used.

Furthermore, a comparable texture was produced in the edge areas and the centers of the magnet material in all tests. In this, the c-axes of the Pr/NdFeB unit cell were preferably perpendicular and rotated with respect to the extrusion direction. Purely radial anisotropy of the magnet material could not be generated.

In summary, it can be assumed that the excessive temperature gradient between the tools and the magnetic billet led to an unfavorable cooling for the process. For further tests, it is useful to develop a concept that allows higher operating temperatures to be realized for the tools in order to counteract the decrease in Temperature of the magnetic material during extrusion. In addition, to enhance shear and thus anisotropy, an increase in the extrusion ratio may be considered.

References

[1] O. Gutfleisch, Controlling the properties of high energy density permanent magnetic materials by different processing routes, J. Phys. D: Appl. Phys. 33 (2000). https://doi.org/10.1088/0022-3727/33/17/201

[2] N.A. Dormidontov, A.G. Dormindontov, A.S. Lileev, A.V. Kamynin, A.A. Lukin, Effect of partial substitution of neodymium with praseodymium on the magnetic and process properties of sintered magnets of type NdFeB, Metal Sci. Heat Treat. 58 (2017) 608-613. https://doi.org/10.1007/s11041-017-0064-6

[3] S. Hirosawa, Y. Matsuura, H. Yamamoto, Magnetization and magnetic anisotropy of $R_2Fe_{14}B$ measured on single crystals, J. Appl. Phys. 59 (1986) 873-879. http://doi.org/10.1063/1.336611

[4] I. Poenarua, A. Lixandrua, S. Riegg, Ce and La as substitutes for Nd in $Nd_2Fe_{14}B$-based melt-spun alloys and hot-deformed magnets: a comparison of structural and magnetic properties, J. Magn. Magn Mater. 478 (2019) 198-205. https://doi.org/10.1016/j.jmmm.2019.01.095

[5] Y. Une, M. Sagawa, Enhancement of coercivity of Nd-Fe-B sintered magnets by grain size reduction, J. Japan Inst. Met. Mater. 76 (2012) 12-16.

[6] J. Liu, H. Sepehri-Amin, T. Ohkubo, Grain size dependence of coercivity of hot-deformed Nd–Fe–B anisotropic magnets, Acta Mater. 82 (2015) 336-343. https://doi.org/10.1016/j.actamat.2014.09.021

[7] L. Li, C.D. Graham, Mechanism of texture formation by hot deformation in rapidly quenched FeNdB, J. Appl. Phys. 67 (1990) 4756-4758. https://doi.org/10.1063/1.344776

[8] R.K. Mishra, E.G. Brewer, R.W. Lee, Grain growth and alignment in hot deformed Nd-Fe-B magnets, J. Appl. Phys. 63 (1988) 3528-3530. https://doi.org/10.1063/1.340731

[9] R. Shioi, H. Miyawaki, T. Morita, Orientation mechanism of hot-deformed anisotropic RE-Fe-B magnets, Denkiseiko 82 (2011) 31-37.

[10] R.K. Mishra, T.Y. Chu, L.K. Rabenberg, The development of the microstructure of die-upset Nd-Fe-B magnets, J. Magn. Magn. Mater. 84 (1990) 88-94. https://doi.org/10.1016/0304-8853(90)90168-P

[11] J. Liu, H. Sepehri-Amin, T. Ohkubo, Microstructure evolution of hotdeformed Nd-Fe-B anisotropic magnets, J. Appl. Phys. 115 (2014) 17A744. https://doi.org/10.1063/1.4867960

[12] R.K. Mishra, Microstructure of hot-pressed and die-upset NdFeB magnets, J. Appl. Phys. 62 (1987) 967-971.
[13] Information on http://www.shinetsu-rare-earth-magnet.jp/e/masspro/
[14] M. Bauser, G. Sauer, K. Siegert, Strangpressen, Aluminium-Verlag, Düsseldorf, 2 Edition, 2001